THE PROTEIN SOCIETY

Crystal structure of AdoMet radical enzyme 7-carboxy-7-deazaguanine synthase from *Escherichia coli* suggests how modifications near [4Fe–4S] cluster engender flavodoxin specificity

Tsehai A.J. Grell,[1] Benjamin N. Bell,[3†] Chi Nguyen,[1,2,3] Daniel P. Dowling,[2,3‡] Nathan A. Bruender,[4§] Vahe Bandarian,[4] and Catherine L. Drennan [1,2,3]*

[1]Department of Chemistry, Massachusetts Institute of Technology, Cambridge, Massachusetts, 02139
[2]Howard Hughes Medical Institute, Massachusetts Institute of Technology, Cambridge, Massachusetts, 02139
[3]Department of Biology, Massachusetts Institute of Technology, Cambridge, Massachusetts, 02139
[4]Department of Chemistry, University of Utah, Salt Lake City, Utah, 84112

Received 5 July 2018; Accepted 15 October 2018
DOI: 10.1002/pro.3529
Published online 00 Month 2018 proteinscience.org

Abstract: **7-Carboxy-7-deazaguanine synthase, QueE, catalyzes the radical mediated ring contraction of 6-carboxy-5,6,7,8-tetrahydropterin, forming the characteristic pyrrolopyrimidine core of all 7-deazaguanine natural products. QueE is a member of the *S*-adenosyl-L-methionine (AdoMet) radical enzyme superfamily, which harnesses the reactivity of radical intermediates to perform challenging chemical reactions. Members of the AdoMet radical enzyme superfamily utilize a canonical binding motif, a $CX_3CX\phi C$ motif, to bind a [4Fe-4S] cluster, and a partial $(\beta/\alpha)_6$ TIM barrel fold for the arrangement of AdoMet and substrates for catalysis. Although variations to both the cluster-binding motif and the core fold have been observed, visualization of drastic variations in the structure of QueE from *Burkholderia multivorans* called into question whether a re-haul of the defining characteristics of this superfamily was in order. Surprisingly, the structure of QueE from *Bacillus subtilis* revealed an architecture more reminiscent of the classical AdoMet radical enzyme. With these two QueE structures revealing varying degrees of alterations to the classical AdoMet fold, a new question arises: what is the purpose of these alterations? Here, we present the structure of a third QueE enzyme from *Escherichia coli,* which establishes the middle range of the spectrum of variation observed in these homologs. With these three homologs, we compare and contrast the structural architecture and make hypotheses about the role of these structural variations in binding and recognizing the biological reductant, flavodoxin.**

Additional Supporting Information may be found in the online version of this article.

Grant sponsor: National Science Foundation 1122374; Grant sponsor: National Institutes of Health R35 GM126982 R01 GM72623 R35 GM126956 and R35 GM126982; Grant sponsor: Helen Hay Whitney. Grant sponsor: CLD is a Howard Hughes Medical Institute Investigator.

*Correspondence to: Catherine L. Drennan, Departments of Biology and Chemistry, Massachusetts Institute of Technology, Cambridge, MA 02139, USA. E-mail: cdrennan@mit.edu

†Current address: Department of Molecular and Cellular Physiology, Stanford University, Palo Alto, California, 94305, USA.

‡Current address: Department of Chemistry, University of Massachusetts–Boston, 100 Morrissey Blvd, Boston, Massachusetts, 02125, USA.

§Current address: Department of Chemistry and Biochemistry, St. Cloud State University, 720 Fourth Avenue S, St. Cloud, Minnesota, 56301, USA.

Broader impact statement: We know more about how enzymes are tailored for catalytic activity than about how enzymes are tailored to react with a physiological reductant. Here, we consider structural differences between three 7-carboxy-7-deazaguanine synthases and how these differences may be related to the interaction between these enzymes and their biological reductant, flavodoxin.

Keywords: AdoMet radical enzymes; flavodoxin; physiological reductant; iron–sulfur clusters; flavin mononucleotide

Introduction

Reduction by low potential electrons is required for the activity of a number of metalloenzymes, including the cobalamin-dependent enzyme methionine synthase[1] and proteins within the 100,000-membered *S*-adenosyl-L-methionine (AdoMet) radical enzyme superfamily.[2] AdoMet radical enzymes utilize the reductive cleavage of a molecule of AdoMet ligated to a [4Fe-4S] cluster to initiate radical chemistry [Fig. 1(A)].[3] The highly reactive intermediate that is generated, 5′-deoxyadenosyl radical or 5′-dAdo•, can abstract a hydrogen-atom (H-atom) from diverse substrates, initiating a variety of chemically challenging and complex reactions.[3,4] This radical generation requires reduction of the AdoMet radical [4Fe-4S] cluster from a resting oxidation state of +2 to +1. The biological reductant, flavodoxin, was first shown to be capable of this reduction in studies of pyruvate formate-lyase activating enzyme.[2] Subsequently, *Escherichia coli* flavodoxin (*Ec*FldA) has been employed as a reductant for a number of AdoMet radical enzymes via an NADPH-dependent flavodoxin reductase system[5–11] [Fig. 1(B)].

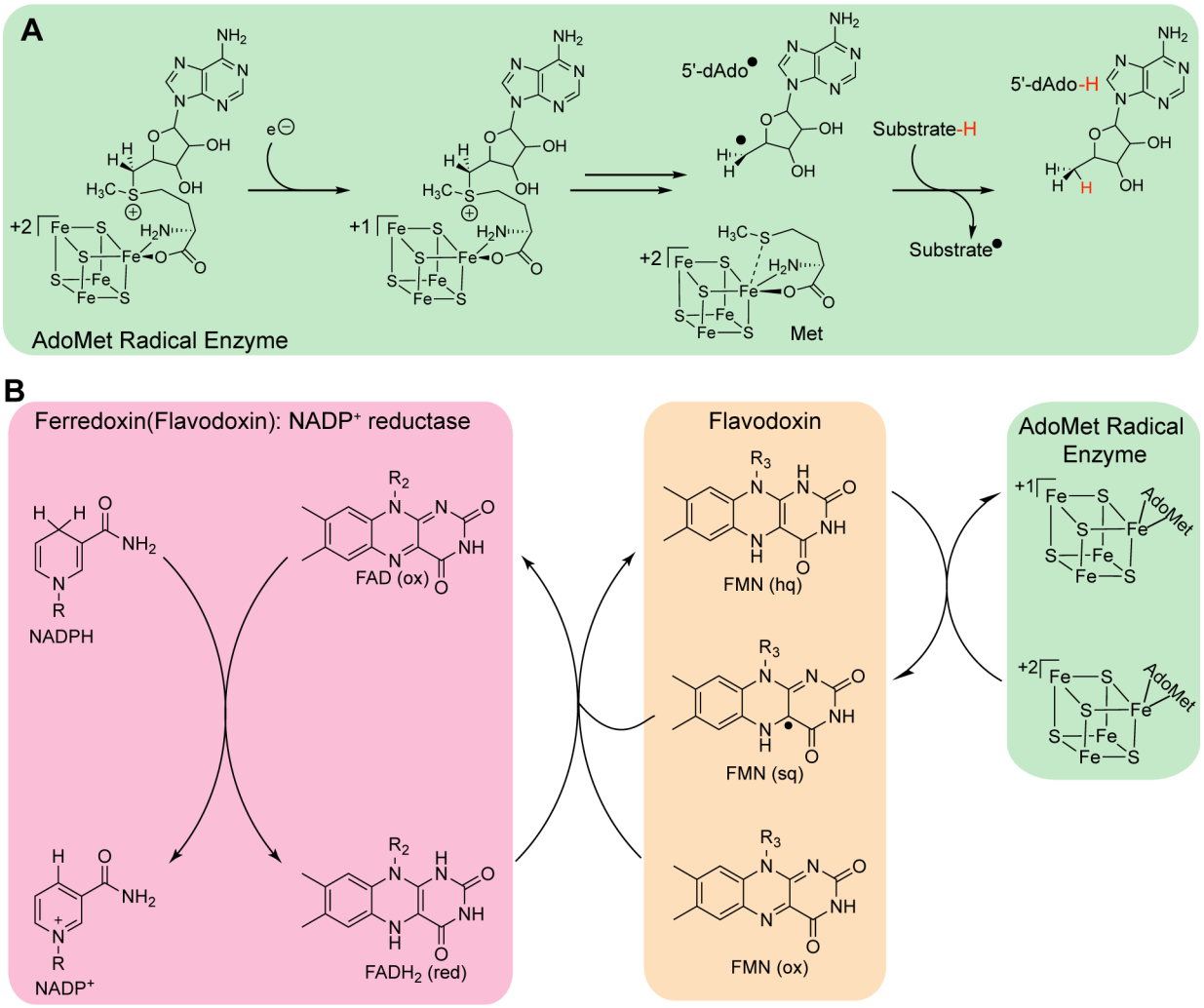

Figure 1. Flavodoxin reduces the AdoMet radical cluster. (A) To initiate radical chemistry through reductive cleavage of AdoMet, the AdoMet radical cluster needs to first be reduced from the resting +2 oxidation state to the +1 oxidation state. (B) Low potentials electrons from NADPH are transferred to the AdoMet radical cluster through the action of Ferredoxin (flavodoxin): $NADP^+$ reductase/Flavodoxin system. Functional parts of NADPH, FAD and FMN are shown.

In addition to the biological *Ec*FldA-flavodoxin reductase system, dithionite can be used to provide reducing equivalents to AdoMet radical enzymes in vitro. In fact, in working with two anaerobic sulfatase enzymes, AtsB and anSME from *Klebsiella pneumonia* and *Clostridium perfringens,* respectively, Grove et al. noted that dithionite appeared to be the more robust reductant in that it increases activity 10–100 fold when compared to *Ec*FldA-flavodoxin reductase.[12,13] Similarly, more product is observed when dithionite instead of *Ec*FldA is used to reduce 7-carboxy-7-deazaguanine synthase (QueE) from *Burkholdeira multivorans* (*Bm*QueE).[14] Interestingly, the QueE from *Bacillus subtilis* (*Bs*QueE) shows the opposite trend from *Bm*QueE, with more product, 7-carboxy-7-deazaguanine (CDG), observed upon incubation with the *Ec*FldA-flavodoxin reductase system compared to dithionite.[15,16] However, maximal production of CDG was observed for *Bs*QueE in the presence of the native flavodoxins, YkuN and YkuP.[15] Taken together these results underlie the need to understand the protein–protein interactions that occur between AdoMet radical enzymes and flavodoxins to begin to dissect the determinants for activation.

Here, we use the highly structurally divergent QueE enzyme family (Fig. 2) as our model system to investigate the hypothesis that the structures of AdoMet radical enzymes are tailored to make specific protein–protein interactions with particular flavodoxins. QueE enzymes are part of the biosynthetic pathway of 7-deazapurine natural products (Fig. SI). They catalyze the radical-mediated ring contraction of 6-carboxy-5,6,7,8-tetrahydropterin (CPH_4) (Fig. 2), forming the characteristic pyrrolopyrimidine core of all 7-deazaguanine natural products, including the modified tRNA nucleoside queuosine[17]. Structures of two QueE homologs have been previously determined (*Bm*QueE and *Bs*QueE)[14,18] and here we present a third structure, that of QueE from *E. coli* (*Ec*QueE) (Table S1). Interestingly, the structure of *Bm*QueE revealed drastic deviations to the AdoMet radical core fold and the cluster-binding motif: *Bm*QueE folds into a pared-down partial (β_6/α_3) TIM barrel, in comparison to the classic partial $(\beta/\alpha)_6$ TIM barrel, and contains a modified cluster-binding motif, a $CX_{14}CX\phi C$ motif,[14] compared to the classic $CX_3CX\phi C$ motif where ϕ is a conserved aromatic residue. In contrast, *Bs*QueE adopts a partial (β_6/α_5) TIM barrel fold with minimal variations from the classic AdoMet radical fold and

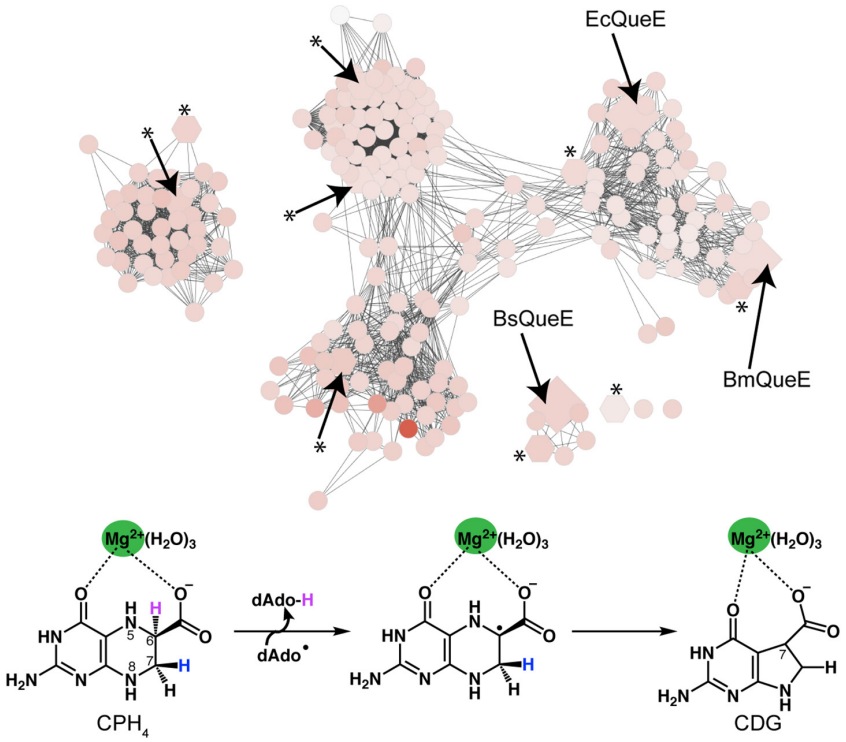

Figure 2. Sequence similarity network of the AdoMet radical enzyme subfamily, 7-carboxy-7-deazaguanine synthases (QueE). The protein sequence similarity network[38] for the QueE AdoMet radical subfamily was obtained from the Structure Function Linkage Database (http://sfld.rbvi.ucsf.edu/django) and visualized in Cytoscape.[39] Each node represents sequences that share 50% identity or higher and node connections are filtered at a Blast Probability of 10^{-25}. Nodes are colored based on increasing sequence length; White nodes denote the shortest sequences (149 amino acids) and the orange node denotes the longest sequence (509 amino acids). *B. multivorans*, *B. subtilis* and *E. coli* QueE sequences are shown as diamonds and sequences used in the sequence alignment (Fig. S2) are shown as hexagons and designated with an asterisk (*). QueE catalyzes the AdoMet and magnesium dependent rearrangement of 6-carboxy-5,6,7,8-tetrahydropterin, CPH_4, to 7-carboxy-7-deazaguanine, CDG.

contains the standard $CX_3CX\phi C$ cluster-binding motif (Fig. S2).[18] *Ec*QueE, as described below, falls in between these two extremes. Given that the flavin mononucleotide (FMN) cofactor of flavodoxin must be within electron transfer distance from the AdoMet radical cluster for cluster reduction,[19–21] we consider how these variations in protein folds observed in these QueE structures could explain the reductant specificity noted above for QueE enzymes.

Results

Ec*QueE reveals an intermediary structure between* Bm*QueE and* Bs*QueE*

The QueE homolog from *E. coli* (*Ec*QueE) was produced in *E. coli* and its ability to convert CPH_4 to CDG was confirmed in preliminary HPLC studies of the purified recombinant protein. The crystal structure of *Ec*QueE was determined to 2.1-Å resolution by multi-wavelength anomalous dispersion (MAD) phasing and R_{work} and R_{free} of 0.205 and 0.238, respectively (Table S2). In the final structure, electron density was observed for most of the crystallization construct with the exception of the first nine residues of the N-terminal hexahistidine tag (His_6tag), residues 192–196 and the final 10 residues. *Ec*QueE folds into a structural and functional head-to-tail homodimer, reminiscent of the published QueE structures from *Burkholderia multivorans* (*Bm*QueE) and *Bacillus subtilis* (*Bs*QueE)[14,18] [Fig. 3(A)]. The overall structure of *Ec*QueE is similar to that of *Bm*QueE (rmsd 1.8 Å) and *Bs*QueE (rmsd 2.9 Å), with variations in the structure and orientation of the loops and α-helices [Fig. 3(B)].

All three QueE homologs fold into variants of the AdoMet radical core domain with extensions at the N- and C-termini. The N-terminal extensions of QueE structures comprise a single anti-parallel β-strand, β1′ [Fig. 4(A–C)], which is found adjacent to β1 of the AdoMet radical core. In *Ec*QueE, the linker and the first residue of the His_6tag are visible, forming an additional α-helix, α1′, at the N-terminus of the enzyme [Fig. 4(A)]. The C-terminal regions of *Bm*QueE and *Bs*QueE fold into a β-strand/α-helix (β7′/α7′) pair, where the β7′ is found adjacent to β6 [Fig. 4(B) and (C)]. In the *Ec*QueE structure, α7′ of the β7′/α7′ pair is not visible due to disorder of the final 10 amino acids of the protein [Fig. 4(A)]. The N- and C-terminal extensions are important for both substrate binding and dimerization in *Bm*QueE and *Bs*QueE[14,18] and it is expected that they will serve the same function in *Ec*QueE. Mutual interactions between the β1′-loop-β1 and β7′ of the adjacent QueE monomers create a dimeric interface such that the β-strands of the N- and C-terminal extensions not only extend the monomeric inner face, but also form an inter-monomer 10-stranded β-sheet that is thought to resemble a crown [Fig. 4(A–C)].

The core of the QueE homolog structures adopt three unique partial TIM barrel folds, where each variant differs in the number and type of α-helices flanking the conserved parallel β-sheet. The previously published structure of *Bm*QueE shows the greatest variation of the three homologs and of the whole AdoMet radical superfamily characterized to date.[20,22] *Bm*QueE sports a vastly pared down AdoMet radical fold, a β_6/α_3, where short loops, L3 and L4, replace α3 and α4 and a short 3_{10}-helix, 3_{10}H5,

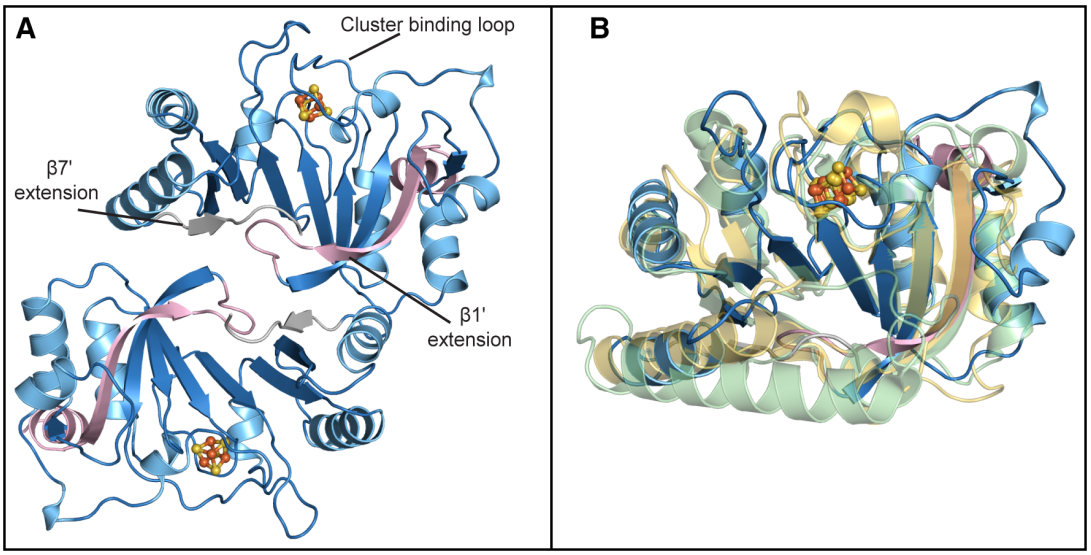

Figure 3. Structure of QueE from *Escherichia coli.* (A) Structure of *Ec*QueE, shown as ribbons, folds into a head-to-tail functional dimer with the dimer interface composed of interactions between the N-terminal (light pink) and C-terminal (grey) extensions. The modified AdoMet core, a partial (β_6/α_5) TIM barrel, is shown in blue. (B) *Ec*QueE (blue) monomer overlays well with the monomers of *Bs*QueE, (PDB ID 5TH5), (translucent light green) and *Bm*QueE, (PDB ID 4NJI), (translucent yellow). In both panels, [4Fe–4S] clusters are shown in a ball and stick representation, where iron is colored orange and sulfur is colored yellow.

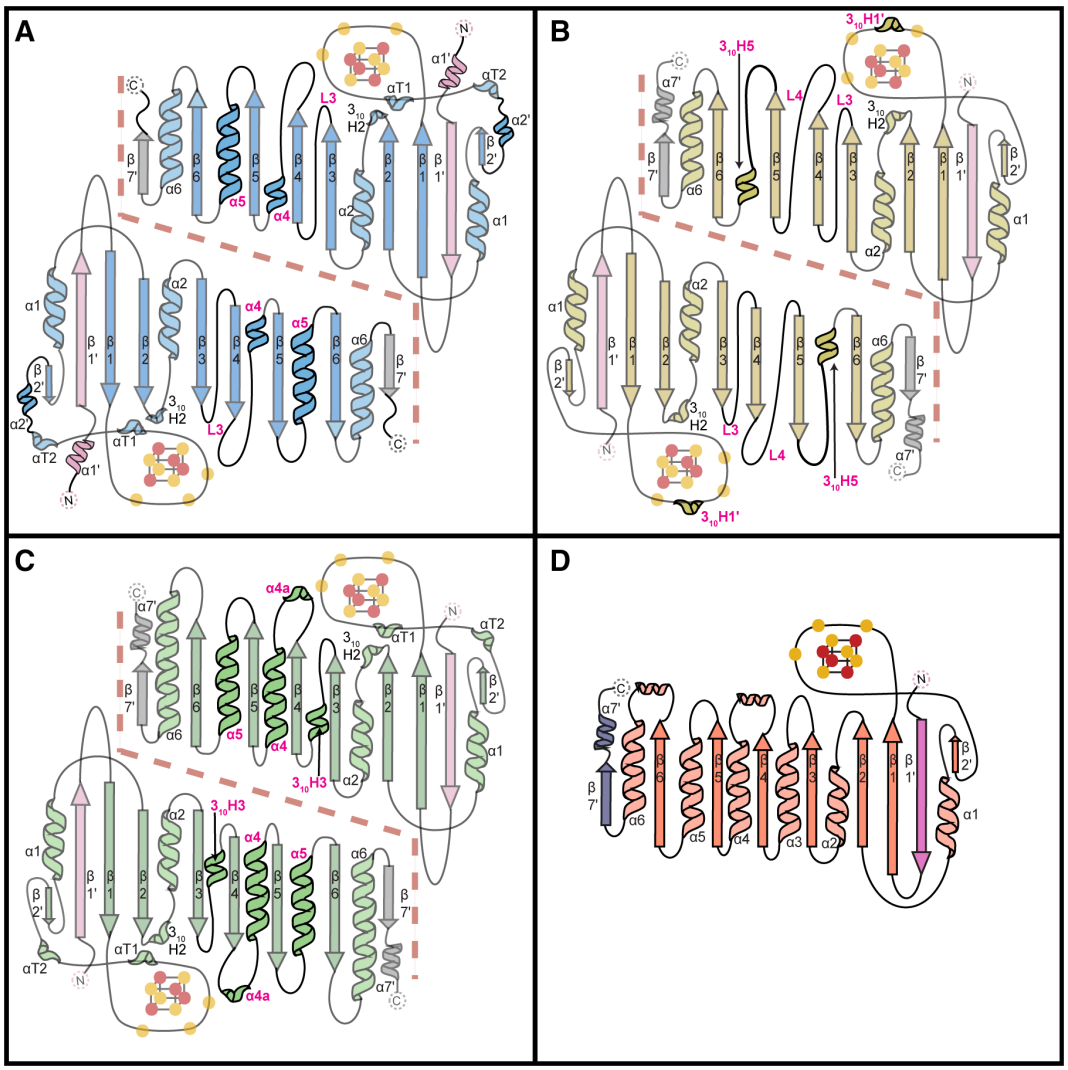

Figure 4. Topology diagrams for QueE homologs and PFL-AE. (A) *Ec*QueE, (B) *Bm*QueE, (C) *Bs*QueE and (D) PFL-AE. The core AdoMet domains are colored blue for *Ec*QueE, yellow for *Bm*QueE and green for *Bs*QueE whereas the N- and C-terminal extensions are colored light pink and grey (respectively) for all three QueE structures. The differences between the QueE homologs structures are shown in bold and the corresponding secondary structure element denoted in magenta and the dashed line delineates the QueE dimer interface. The topology diagram of PFL-AE is shown with the N- and C-terminal extensions colored pink and slate respectively and AdoMet domain colored in coral. The iron atoms of the [4Fe–4S] clusters are colored orange and sulfur atoms are colored yellow. Cysteine ligands to the [4Fe–4S] cluster are shown as yellow circles. Structural elements outside the AdoMet radical core fold are labeled with a prime.

replaces α5 [Fig. 4(B)]. The variations in the AdoMet radical core of *Bs*QueE are the most conservative of the three homologs. *Bs*QueE folds into a partial β_6/α_5 TIM barrel, which contains a non-traditional short 3_{10}-helix, 3_{10}H3 in place of α3 [Fig. 4(C)]. Similarly, the AdoMet radical domain of *Ec*QueE folds into a partial β_6/α_5 TIM barrel with a variation at the α3 position, but this change is not as conservative as that seen in *Bs*QueE [Fig. 4(A)]. In *Ec*QueE, α3 is replaced by a short loop (L3), reminiscent of the α3 alternative in *Bm*QueE, and also has a long loop connecting β4 to a very short α4.

The three QueE homologs, to date, are the smallest structurally characterized AdoMet radical enzymes, with *Bm*QueE spanning only 210 amino acid residues, *Ec*QueE, 223 amino acid residues and *Bs*QueE 243 amino acid residues. The second smallest non-QueE AdoMet radical enzyme structurally characterized, PFL-AE (246 amino acid residues), shows surprising structural similarities to the QueE homologs, in particular *Bs*QueE. PFL-AE adopts a normal AdoMet radical core,[21] a $(\beta/\alpha)_6$ TIM barrel, and contains N- and C-terminal extensions, β1′ and β7′, which closely resemble those found in QueE [Fig. 4(D)]. Unlike QueE, PFL-AE is a monomer, thus these terminal extensions do not play a role in oligomerization. However, similar to QueE, the N-terminal extension is involved in substrate binding.[21]

In all three QueE structures, electron density was present for a [4Fe–4S] cluster bound by three cysteine ligands, leaving a site-differentiated iron. Sequence analysis revealed an 11 amino acid insertion in the

cluster-binding loop of *Bm*QueE, resulting in a $CX_{14}CX\phi C$ sequence instead of the canonical $CX_3CX\phi C$ cluster-binding motif. Surprisingly, the insertion did not affect cysteine positioning and cluster binding and the cysteine ligands from the cluster binding loop superimposed well with other AdoMet radical enzymes [Fig. 3(B)]. Instead, the insertion folds into a short 3_{10}-helix, 3_{10}H1, found on top of the AdoMet radical cluster [Fig. 4(B)] and further sequesters the cluster from solvent as well as increases the negative charge in that area. Following the cluster-binding motif in *Bm*QueE, the loop folds into a short β-strand, β2′, before transitioning into α1, another structural addition outside of the AdoMet radical core. Sequence and structural analysis of *Bs*QueE and *Ec*QueE show a canonical cluster binding loop motif, $CX_3CX\phi C$, which positions the cluster at the top of the AdoMet radical barrel (Figs. 3 and 4). Akin to *Bm*QueE, the transition in *Ec*QueE and *Bs*QueE from the cluster-binding motif to α1 involves additional structural elements, a short α-helix α2′ and/or helical turns αT1 and αT2, respectively, which precede β2′ and the subsequent α1 of the AdoMet radical core [Fig. 4(A) and (C)].

AdoMet binding motifs appear conserved in the QueE homologs

Structural analyses of AdoMet radical enzymes have revealed a number of structural motifs for securing AdoMet in position with respect to the [4Fe–4S] cluster for radical generation.[20,22] Structures of *Bm*QueE with AdoMet bound (Table S1) revealed that alterations in the core fold and cluster-binding motif, which were observed in that enzyme, did not lead to changes in the way that the enzyme bound AdoMet; AdoMet binding motifs were conserved [Figs. 5(A), S2, and S3].[14] Likewise, a structure of *Bs*QueE bound to an AdoMet-derived adduct, 6-carboxypterin-5′-deoxyadenosyl (6-CP—dAdo) (Table S1), indicated conservation of AdoMet binding motifs [Figs. 5 (B) and S2].[18] Despite considerable effort, no structure of *Ec*QueE has been obtained bound to either AdoMet or an AdoMet-derived adduct, however, structural comparisons suggest that AdoMet-binding residues are conserved (Figs. 5, S2, and S3). Interestingly, these residues in *Ec*QueE are not pre-organized for AdoMet binding. Modeling of AdoMet into the *Ec*QueE active site [Figs. 5(C) and S3] indicates that side chain rearrangements will need to occur. No other QueE enzyme has been captured without a ligand bound (Table S1), thus the *Ec* structure is the first to show that the QueE active site is not pre-organized to bind AdoMet.

Substrate binding motifs appear conserved among QueE homologs

Structures of *Bm*QueE have been determined that depict the binding sites for substrate CPH_4, product CDG, and the catalytically essential Mg^{2+} ion (Table S1). Given that analogous structures could not be obtained for the *Bs* and *Ec* enzymes, we used a *Bm*QueE structure (PDB ID 4NJI) [Fig. 6(A) and (D)] to model substrate binding to *Bs*QueE [Fig. 6(B) and (E)], and to *Ec*QueE [Fig. 6(C) and (F)].[14,18] The QueE active site is found in the lateral opening of the partial TIM barrel and consists of residues from the AdoMet radical core and N- and C-terminal extensions. The pterin ring of substrate is oriented in the active site through several interactions, including π-π stacking with His and Phe residues in both *Bm*QueE and *Bs*QueE. In the *Ec*QueE structure, T_{216} appears to be

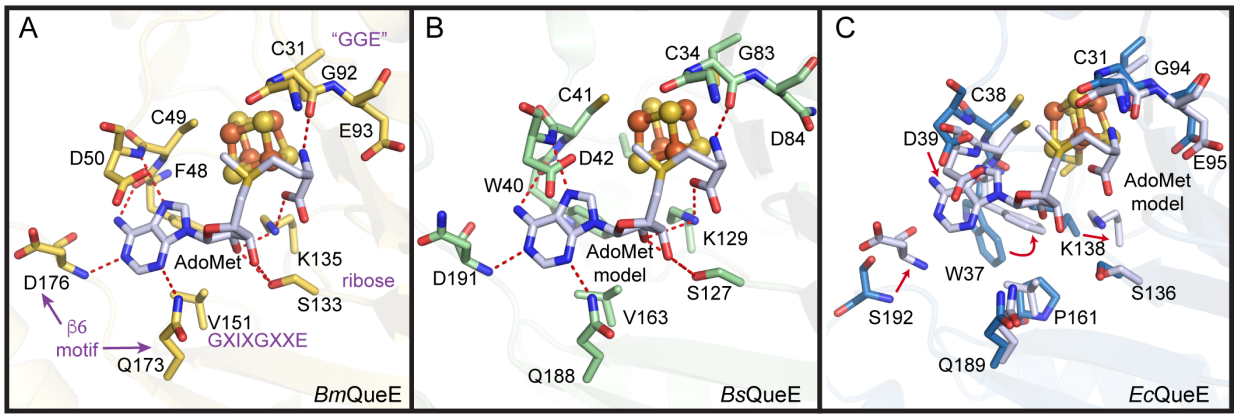

Figure 5. AdoMet binding pocket in QueE homologs. AdoMet binding within the AdoMet core (translucent ribbons) is shown for (A) *Bm*QueE (PDB ID 4NJI), (B) *Bs*QueE (PDB ID 5TH5) and (C) *Ec*QueE. In (A), AdoMet binding motifs are labeled in magenta. See Fig. S3 for stereo views and further description of AdoMet binding. The binding pockets are composed of residues (sticks), which can provide hydrogen bonds (red) to AdoMet (white). The irons (orange) and the sulfurs (yellow) of the [4Fe-4S] AdoMet radical cluster are shown as spheres. In (B), the intact AdoMet molecule is modeled using the adenosyl moiety of the 6-carboxypterin-5′-deoxyadenosyl ester adduct (PDB ID 5TH5) and an intact AdoMet molecule (PDB ID 4NJI) as a guide. The AdoMet binding pocket of *Ec*QueE (blue) is shown overlaid with the binding pocket from *Bm*QueE (white) to highlight the changes that need to be made (red arrows) to allow binding of the modeled AdoMet (white) molecule.

oriented to in place of these π–π stacking interactions with the substrate, but it is difficult to tell if this will remain true once substrate binds as the residues following T_{216}, which includes H_{217}, are disordered. In addition, the disordered C-terminus does not allow for visualization of the C-terminal plug in *Ec*QueE, which is provided by the carboxylate moiety of the final residue of the protein, P_{210} in *Bm*QueE or V_{243} in *Bs*QueE. These C-terminal residues provide interactions to the N2 exocyclic amino group, N3 and the C4 carbonyl group, whereas residues R_{27} and T_{90} in *Bm*QueE, R_{30} and S_{81} in *Bs*QueE, and possibly R_{27} and T_{92} in *Ec*QueE position the C6 carboxyl group. Hydrogen bonds from the backbone of N-terminal residues, G_{14} and L_{12} in *Bm*QueE and *Ec*QueE and G_{17} and Ile_{15} in *Bs*QueE, further position substrate in the active site (Fig. 6). All QueE homologs tested require Mg^{2+} for catalysis,[14] and the structure of *Bm*QueE revealed its binding site [Fig. 6(A) and (D)]. Only one residue, T_{51} (*Bm*QueE), directly interacts with the catalytic metal, Mg^{2+}, and residues D_{50} and H_{204} (*Bm*QueE) indirectly interact with the Mg^{2+} through water molecules [Fig. 6(D)]. Corresponding residues are S_{43}, D_{42}, and H_{223} in *Bs*QueE [Fig. 6(E)] and with rearrangement upon ligand binding, T_{40}, D_{39}, and T_{216} in *Ec*QueE [Fig. 6(F)]. Although *Bs* and *Ec* QueE structures do not have Mg^{2+} bound, water molecules are present in these structures that are already positioned for interaction with Mg^{2+}.

Ec*QueE and* Ec*FldA show surface charge–charge complementarity*

Flavodoxins are small (~20 kDa) FMN-containing proteins with limited sequence conservation (Fig. 7), but with a shared overall structural fold. They use a Rossmann-like fold with a five-stranded parallel β-sheet that is surrounded by five helices (Figs. 7 and 8)[23] to bind their cofactor FMN. Although no structure of a flavodoxin bound to an AdoMet radical enzyme has been determined, flavodoxin must make protein–protein contacts with the AdoMet radical enzyme in the vicinity of its [4Fe–4S] cluster to afford for facile electron transfer.[24]

Electrostatics are a major driving force in protein–protein interactions, therefore we calculated the electrostatic surfaces for both our structure of *Ec*QueE and the published structure of *Ec*FldA.[25] The surface of *Ec*QueE is mainly negative with a positive strip running along the "top" of the partial TIM barrel, i.e. at C-terminal ends of β-strands where the cluster-binding loop (CBL) and [4Fe–4S] cluster reside (Fig. 8). This "top positive patch" is made up of residues from α2′, the CBL, and the loop between β4 and the shortened α4 (Loop 4), the loop between β5 and α5 and the loop between β6 and α6 (Fig. 8). Another area with a positive electrostatic surface is found on the back side of the AdoMet radical barrel, made up of residues from the loop between α1′ and β1′ and the loop between β2 and α2.

The electrostatic surface of *Ec*FldA is also largely negative (Fig. 8) with one major positive patch of electrostatic surface on the opposite side of the FMN binding pocket, corresponding to residues 20–30 and residues from the C-terminal region. The electrostatic surface surrounding the FMN cofactor is negative and is therefore complementary to the large positive patch composed chiefly of residues from CBL and Loop 4 [Fig. 8(B)].

In addition to this charge complementary between the surface of the [4Fe–4S] cluster binding region of *Ec*QueE and the surface of *Ec*FldA, there is shape complementarity as well. The surface of *Ec*QueE near the cluster, the "top" patch, appears to be a lock-and-key match with the surface of *Ec*FldA that displays the FMN (Fig. 8).

QueE homologs display variable surfaces

The variations in fold between QueE homologs, from the replacement of helices with loops and the substitutions of long helices with shorter helices or with 3_{10} turns, create a very different overall shape for these QueE enzymes (Fig. 9). *Bs*QueE, which is the most traditional of the three QueEs in terms of the larger AdoMet radical enzyme family, has a monomeric unit whose overall shape is most barrel-like and most spherical [Fig. 9(C)]. In contrast, the shorter helices or lack of helices in *Ec* and *Bm*QueE homologs generate structures that are flatter by comparison with *Bs*QueE (Fig. 9). Additionally, the electrostatic surfaces of these three QueE homologs are quite different (Fig. 9). The electrostatic surface of *Bm*QueE is largely negatively charged with small positively charged patches [Fig. 9(A)]. In contrast, the electrostatic surfaces of the *Bs*QueE [Fig. 9(C)] and *Ec*QueE [Fig. 9(B)] contain considerably larger positive patches. Despite the difference in the sizes of the positive patches, the locations of these patches are similar. All QueEs have a "top" positive patch near the cluster binding loop (CBL), and a "backside" patch that corresponds to loops and α-helices (α5 and α6, in particular) that flank the outside of the barrel (Fig. 9). The "top" patch, which is very large in *Bs*QueE, is created by a number of secondary structural elements that surround the [4Fe–4S] cluster, including the N- and C-terminal ends of the CBL, αT2, β2′, 3_{10}H2, loops following β3 (Loop 3) and β4 (Loop 4), the N-terminal ends of β1′, α2, and α4 and the C-terminal end of α5 [Fig. 9(C)]. In *Ec*QueE, the corresponding "top" positive patch, which is intermediary in size between the *Bm* and *Bs* enzymes, is generated by residues of the CBL, αT1, α2′, the N-terminus of the loop following β4 (Loop 4) and the N-terminal ends of α5 and α6 [Fig. 9(B)].

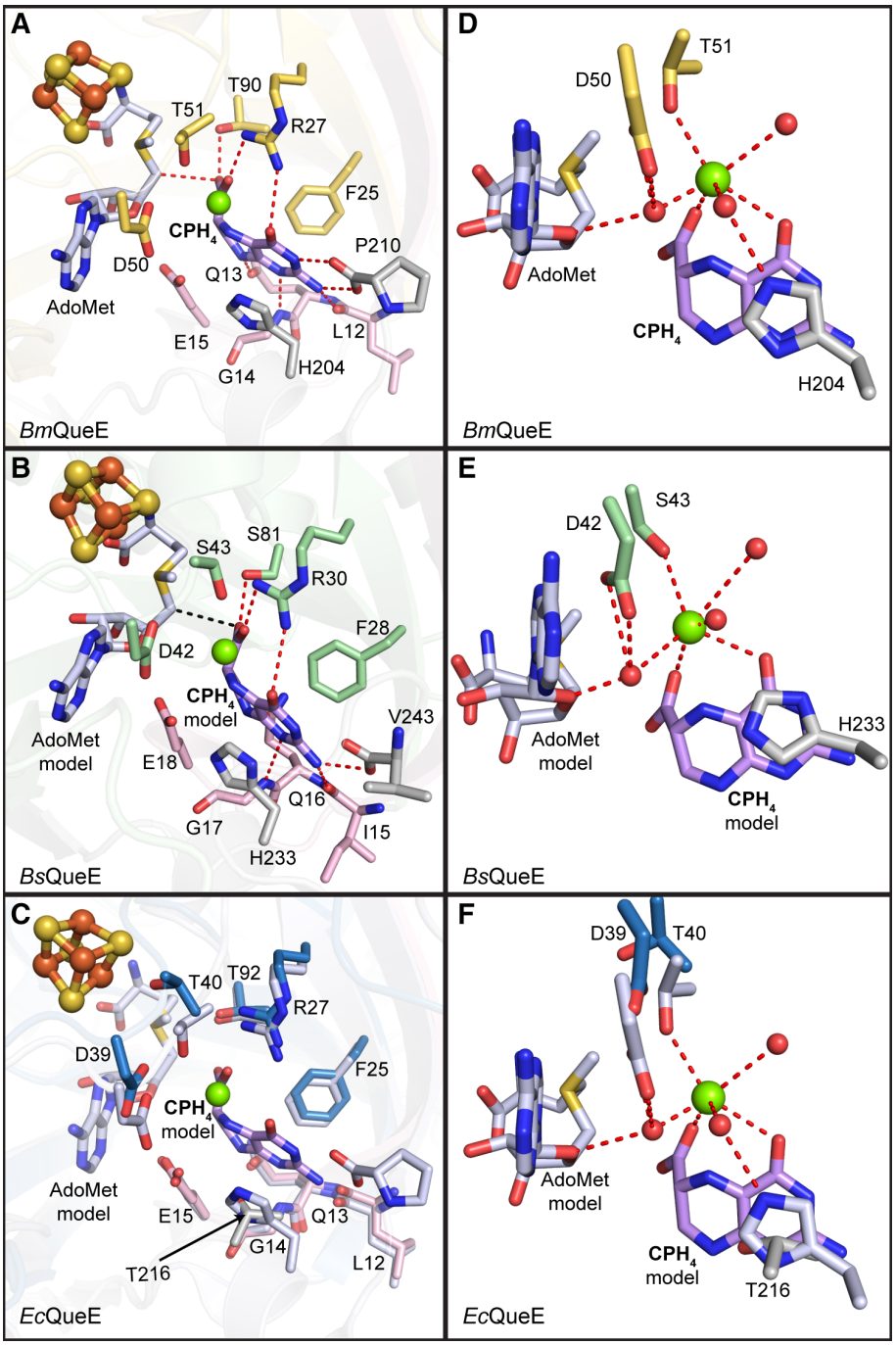

Figure 6. Substrate binding pocket. Residues (in sticks) that comprise the substrate-binding pocket are shown for each of the QueE homologs. (A) CPH_4 is bound to the active site by residues from the N-terminal extension (pink), the AdoMet radical core fold (yellow) and the C-terminal extension (grey) of *Bm*QueE (PDB ID 4NJI). (B) In the modeled orientation, CPH_4 appears to interact with the AdoMet radical domain (green) of *Bs*QueE in addition to the N- and C-terminal extensions, colored pink and grey, respectively. (C) CPH_4 modeled into *Ec*QueE. AdoMet radical domain in blue and N- and C-terminal extensions in pink and grey, respectively, are shown overlaid with the active site of *Bm*QueE (white). (D) CPH_4 binding in *Bm*QueE (PDB ID 4NJI) (yellow) creates a magnesium-binding site. (E) CPH_4 binding in *Bs*QueE (PDB ID 5TH5) (green) is expected to create a magnesium-binding site similar to that seen in *Bm*QueE. (F) The putative magnesium-binding site of *Ec*QueE (blue) is shown overlaid with the CPH_4 bound *Bm*QueE (PDB ID 4NJI) (white). The substrate, CPH_4, is shown in lilac, the catalytically essential magnesium is represented as a green sphere, the irons (orange) and the sulfurs (yellow) of the [4Fe–4S] AdoMet radical cluster are shown as spheres, AdoMet is shown in light blue and hydrogen bonds are shown as red dashes. Water molecules (red spheres) necessary for magnesium binding are shown.

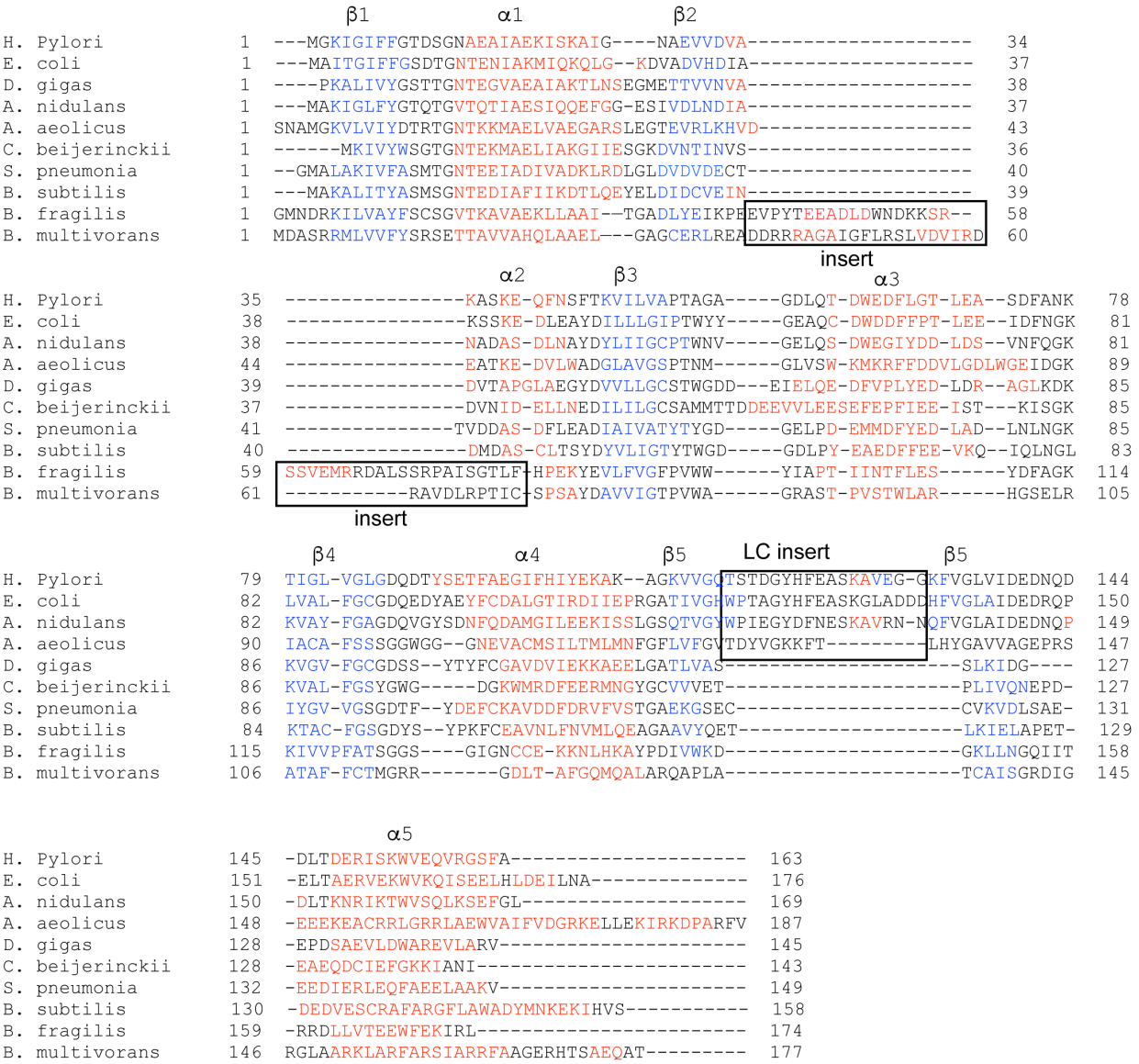

Figure 7. Flavodoxins sequence alignment. Sequences include flavodoxins from *Helicobacter pylori, Escherichia coli, Anacystis nidulans, Aquifex aeolicus, Desulfovibrio gigas, Clostridium beijerinckii, Streptococcus pneumonia TIGR4, Bacillus subtilis* (YkuN), *Bacteroides fragilis NCTC 9343*, and *Burkholderia multivorans.* The sequence alignment is colored according to secondary structure, blue for β-strands and red for α-helices, and the insertion for long chain flavodoxins and the chain insertion in flavodoxins from *B. multivorans* and *B. fragilis* are denoted with a box.

*Bm*QueE's smaller "top" patch is made up of β1′ and β2′, and N- and C-termini of the CBL [Fig. 9(A)].

Discussion

Here, we present the structure of *Ec*QueE in the absence of substrate and compare this structure with previous QueE structures from *Bm* and *Bs*. Interestingly, these three QueEs, which all catalyze the exact same reaction, are farther apart in sequence space than are other AdoMet radical enzymes that catalyze completely different reactions.[14] *Bm*QueE is an outlier in an AdoMet radical enzyme superfamily with a minimal AdoMet core fold of (β_6/α_3) instead of the classic $(\beta/\alpha)_6$ partial TIM barrel fold, but these architectural differences are not required for 7-carboxy-7-deazaguanine synthesis as the enzyme variant from *Bs* has a much more traditional (β_6/α_5) fold.[18] It does not appear that the minimalist *Bm*QueE is a one-off outlier either. If this were the case, we would expect that all other QueE enzymes would look like *Bs*QueE and they do not. This third QueE structure shows that the *Ec* enzyme has a fold that is intermediate between the other two QueEs. Further, the QueE sequence similarity network (SSN) (Fig. 2) suggests that even more variation is likely, with unexplored sequence space appearing to represent QueEs that will be even more distantly related than *Bs*, *Ec*, and *Bm* enzymes are to each other. Interestingly, there are QueEs of various lengths in all of the sequence clusters (Fig. 2), indicating that sequence length and

sequence conservation are not highly correlated. *What is the purpose of this QueE structural diversity?* With the structural data that we now have in hand, we evaluated the relationship between fold variation and AdoMet binding, substrate binding, Mg^{2+} ion binding, and flavodoxin binding, and propose that the QueE structural variation is most likely in response to flavodoxin variations for the reasons outlined below.

Although we were not able to obtain a structure of *Ec* or *Bs*QueEs with AdoMet, structural comparisons suggest that AdoMet binding residues are conserved. The *Ec* structure indicates that residues are not pre-organized to bind AdoMet, but with modest side chain rearrangements, the binding pocket for the AdoMet cofactor is expected to be analogous to that visualized in the *Bm*QueE structure. Similarly, side chain rearrangements are required for CPH_4 binding in *Ec*QueE, but sequence conservation and structural conservation near the active site predict an identical substrate binding mode in *Ec* and in *Bm*QueE. *Bs*QueE is also expected to bind substrate in an analogous fashion.[18] Finally, the binding site for the required Mg^{2+} ion appears to be conserved. Thus, there is no indication that the sequence and structural diversity displayed by the QueE enzyme family is related to cofactor or substrate binding or to any variation in the enzyme mechanism used for 7-carboxy-7-deazaguanine synthesis.

In contrast to the observations about AdoMet, substrate and Mg^{2+} binding, the QueE structures do appear to vary in the surface regions around the [4Fe–4S] cluster where flavodoxin must bind to deliver an electron to initiate radical generation. With the structure of *Ec*FldA known,[25] the determination of the QueE structure from *E. coli* provides the opportunity to evaluate the interaction surfaces for a physiological AdoMet radical enzyme–flavodoxin pair. *Ec*FldA is a small, highly negatively charged protein that contains a partially exposed FMN cofactor, and here we find that *Ec*QueE has a complementary positively charged patch surrounding the [4Fe–4S] cluster binding region (Fig. 9). Most of the rest of the surface of *Ec*QueE is negatively charged, which should restrict non-productive binding events. Additionally, the shape complementarity of the "top" ([4Fe–4S]-cluster binding region) of *Ec*QueE and the FMN-exposed side of *Ec*FldA is remarkable (Fig. 8). Protrusions of the *Ec*FldA surface are matched with indentations in the *Ec*QueE surface. The bringing together of these structurally and electrostatically complementary surfaces will juxtapose the FMN of *Ec*FldA and the [4Fe–4S] cluster of *Ec*QueE, facilitating electron transfer for this physiological redox protein pair.

Interestingly, structural comparisons of the three QueE homologs show substantial differences in shape and charge (Fig. 9). The replacement of helices with loops and variations in helical lengths observed for these QueE enzymes has the net effect of changing the overall shape of the monomeric unit. These structural differences along with sequence variations alter the

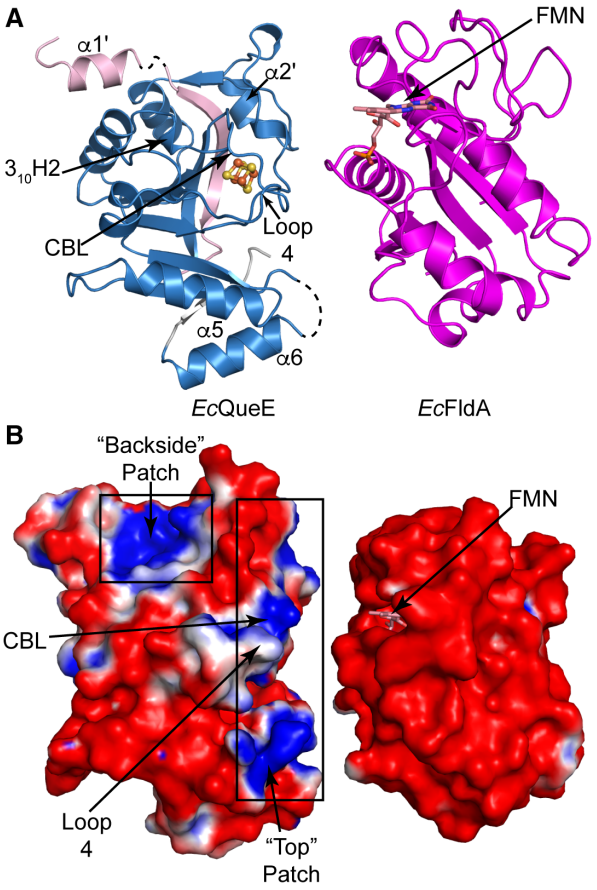

Figure 8. Electrostatic surface charge for *Ec*QueE and the cognate Fld, *Ec*fldA. (A) Ribbon drawing of monomer of *Ec*QueE with the AdoMet radical core in blue and the N- and C-terminals in light pink and grey, respectively, oriented such that the predicted binding sites are facing *Ec*FldA. The structure of *Ec*FldA (PDB ID 1AHN) is also shown in ribbon representation (magenta) with the FMN cofactor and the loops proposed to bind partner proteins facing *Ec*QueE. (B) The solvent accessible electrostatic surface representations of *Ec*QueE and *Ec*FldA with FMN colored salmon are also displayed in the same orientation as in A. Electrostatic potentials are depicted on a colorimetric scale from red to blue for −1 to +1 kTe^{-1}.

electrostatic charge of the resulting surfaces. These structural observations are consistent with the report that *Ec*FldA does not promote the CDG synthesis activity of all three QueEs uniformly. *Ec*FldA works to some degree with *Bs*QueE; it is more effective than chemical dithionite in promoting CDG synthesis, but falls short of the activity observed with the *B. subtilis* partner proteins. *Ec*FldA, on the other hand, is less effective than chemical dithionite in promoting activity of *Bm*QueE.[14,15] In addition to lower turnover numbers when a non-physiological FldA is used, the ratio of AdoMet abortive cleavage events to turnover events also increases.[15] Given the shape differential between *Ec*QueE and *Bs*QueE (Fig. 9), it is a bit surprising that *Ec*FldA is able to work as well as it does. It is likely that the large positively charged patches on *Bs*QueE compensate for imperfect shape complementarity.

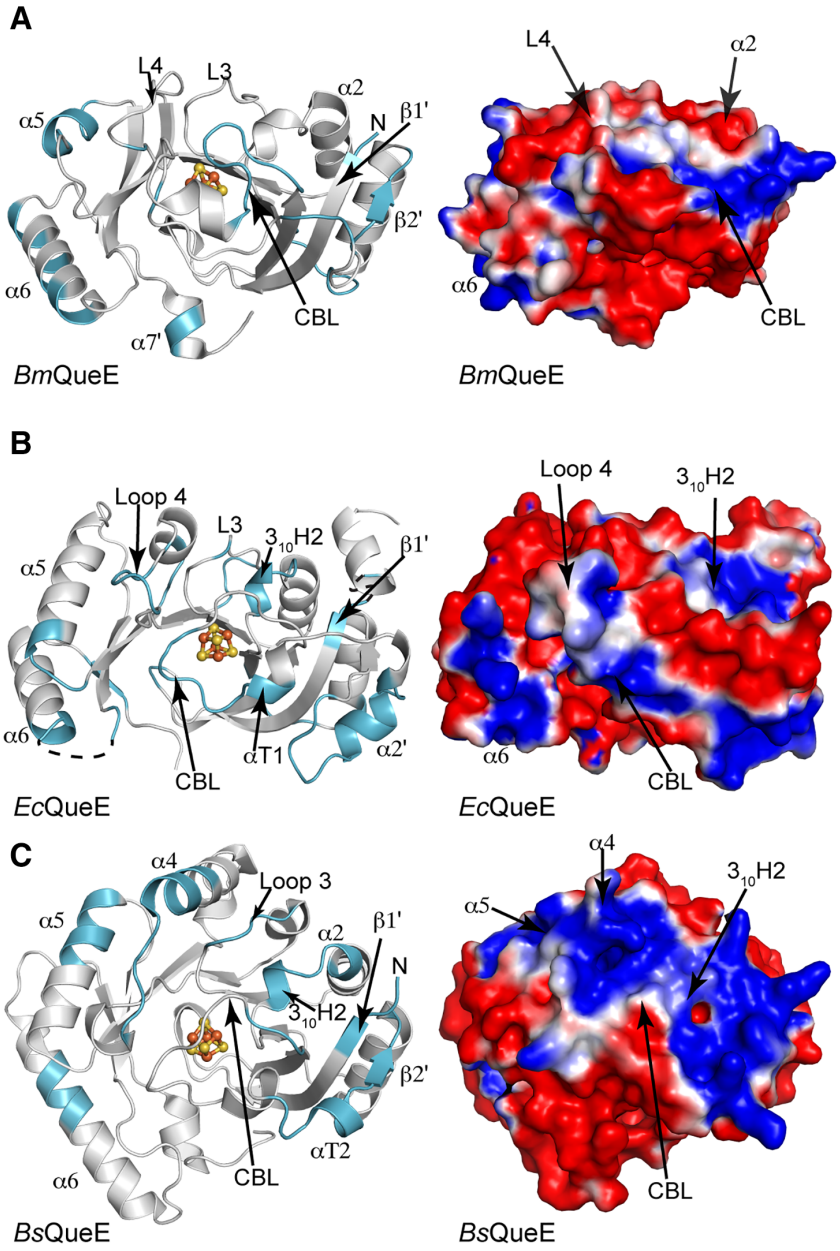

Figure 9. QueE orthologs show differential electrostatic surfaces. Ribbon drawing of QueE orthologs, shown as monomers in grey, with the structural elements contributing to the positive electrostatic surface highlighted in cyan. The electrostatic surface potential is shown colored from red to blue for −1 to +1 kTe^{-1} on the right of each panel for the corresponding orientation of the QueE orthologs. (A) *Bm*QueE, (B) *Ec*QueE, and (C) *Bs*QueE.

*Bm*QueE, in contrast, lacks shape complementarity, lacks the large surface positive charge (Fig. 9) and is not activated to a significant extent by *Ec*FldA. *Bm*QueE is the most negatively charged QueE, and given that flavodoxins tend to be negatively charged, it is tempting to speculate that the cognate *Bm* flavodoxin may be atypical. No structures are known of any of the three flavodoxins from *Bm*, but a sequence of one of the *Bm* flavodoxins that is shown in Figure 7 does suggest that this *Bm*Fld will be unusual. In particular, it has two inserts that are not present in the *Ec*FldA or in most other flavodoxins (Fig. 7). Taken together, these data are in agreement with the idea that structural variations observed in QueEs may be matched with changes to their cognate flavodoxins or other biological reductant. In short, structures of *Ec*QueE and *Ec*FldA help us understand why these partner proteins work well together, and QueE structural comparisons provide explanations of why turnover is lower and abortive cleavage is higher when *Ec*FldA is paired with *Bm*QueE or *Bs*QueE. Structures of flavodoxins from *Bm* will provide further validation of this idea and will allow us to understand how the unusual *Bm*QueE is activated for catalysis *in vivo*.

Conclusion

Although variations to the AdoMet radical core have been observed before outside of the QueE system, these

changes have been attributed to tailoring of the enzyme to the chemistry performed and/or substrate binding. Structural analysis of three QueE homologs, which perform identical chemistry on the same substrate, revealed both structural and electrostatic differences. We believe these variations serve to dictate binding to their cognate biological reductant. Charge–charge complementarity could serve as a hard discriminant, preventing flavodoxins with incompatibly charged surfaces from binding to QueE. Surface complementarity (dictated by the structure) can further fine-tune these interactions, allowing for activation of the enzyme. It is only when there is both charge and surface complementarity that full activation of the enzyme occurs. Thus, we expect some sort of co-evolution of flavodoxins–ligand pairs, to allow for complementarity needed for optimal activation.

Materials and Methods

Preparation of Ec*QueE*

The gene corresponding to QueE was cloned from *E. coli* W3110 into the *Nde*I and *Hind*III sites of pET28a for expression of His_6tagged protein. Expression, purification, reconstitution, and activity assays were carried out as described previously for *Bs*QueE.[16]

Crystallization and data collection of Ec*QueE*

Crystallization conditions for His_6tagged *Ec*QueE were initially identified by sparse matrix screening within a room temperature MBraun anaerobic chamber using a TTP Mosquito pipetting robot and optimized by sitting drop vapor diffusion within a Coy scientific anaerobic chamber. Data quality crystals were obtained by equilibrating drops containing 1.5 μL of protein (10 mg/mL in 50 mM Tris•HCl pH 8.0 and 10 mM dithiothreitol) and 0.5 μL of reservoir (175–200 mM magnesium chloride, 25–30% PEG 400 and 100 mM Tris•HCl pH 8.5) over a reservoir of 500 μL. Brown 200–300 μm × 30 μm rod-like crystals were obtained after 24 h. Crystals were harvested from the mother liquor with no further cryoprotecting and cryo-cooled in liquid nitrogen within the Coy anaerobic chamber.

Diffraction data were collected at the Advanced Photon Source (Argonne, IL) at beamline 24-ID-C, using a Pilatus 6 M pixel detector at 100 K. Data were collected on the same crystal at two different wavelengths. An Fe-peak data set was collected in six 35° wedges using an inverse beam method (Friedel mates were measured consecutively, rotating the crystal 180° every 120 frames with 0.3° oscillation steps and an exposure time of 0.3 s) at a wavelength of 1.7384 Å to 2.6-Å resolution. The remote data set was collected at a wavelength of 0.9792 Å to 2.1-Å resolution, using the continuous vector scan method (the crystal was continuously translated along its major crystallographic axis during data collection). All data were processed in HKL2000[26] in the space group $P2_12_12_1$.

Structure determination and refinement

The structure of *Ec*QueE with two molecules in the asymmetric unit was solved using Fe multi-wavelength anomalous dispersion (MAD) phasing. Two Fe sites were identified with occupancies above 0.9 using the remote and peak data sets trimmed to 4-Å resolution in ShelxD/E[27] in HKL2MAP.[28] Heavy atom site refinement, experimental map generation, automated model building and density modification were performed in SOLVE and RESOLVE in Phenix AutoSol.[29] The figure of merit-weighted electron density map (FOM = 0.64 to 4-Å resolution) obtained was sufficient for tracing protein secondary structure elements manually in Coot. The automated model was extensively rebuilt to produce a model for one monomer in the asymmetric unit. The second monomer was placed in the asymmetric unit using Phenix AutoBuild[30] and the resulting model was subjected to iterative rounds of refinement and density modification using Resolve,[30] and phenix.refine,[31] respectively, and the resolution was extended to the full-length of the data, 2.1-Å resolution. The resulting *R*-factors were 25.6% and 29.9% working and free *R*-factors, respectively.

Iterative rounds of model building in Coot[32] and refinement in Phenix[31] using atomic coordinates, atomic displacement parameters (*B*-factors), and non-crystallographic symmetry (NCS) restraints, without sigma cutoffs, completed the model. In advanced stages of refinement, water molecules were manually added in Coot[32] and in final stages, NCS restraints were released and refinement included translation, libration, screw (TLS) parameterization with one TLS group per monomer. The model was validated using simulated annealing composite omit maps calculated in Phenix. Analysis of geometry using MolProbity[33] indicates that 96.45%, 3.55%, and 0.0% of residues were in the favored, allowed, and disallowed regions of the Ramachandran plot, respectively. The final structure of *Ec*QueE contains 224 residues (out of 243) and a [4Fe-4S] cluster in chain A and 229 residues (out of 243) and a [4Fe–4S] cluster in chain B. In both chains, the His_6tag linker region containing the Tobacco Etch Virus (TEV) protease cleavage site is visible as well as a His residue from the His_6-tag. Crystallography software packages were compiled by SBGrid.[34]

Manual docking of AdoMet and substrates

Docking of AdoMet, and CPH_4 molecules into *Ec*QueE was performed manually in Coot[32] using *Bm*QueE (PDB ID 4NJI) as a guide. In *Bs*QueE (PDB ID 5TH5), 6-CP-dAdo binding foretold the binding interactions of AdoMet and substrate, therefore, the adduct was used, in addition to *Bm*QueE (PDB ID

4NJI), to configure intact AdoMet and CPH_4 in the active site of *Ec*QueE.

Preparation of Figures and electrostatic surfaces

All crystallographic figures were created with PyMOL Software and electrostatic surface potentials were calculated using the Adaptive Poisson–Boltzmann Solver plugin implemented in PyMOL, using default parameters.[35–37]

Acknowledgments

This research was supported by National Institutes of General Medical Sciences of the National Institutes of Health grants R35 GM12682 (awarded to C.L.D.) and R01 GM72623 (awarded to V.B.) with Administrative Supplement GM72623 S01 to V.B. for the collaboration between V.B. and C.L.D, R35 GM126982 (awarded to C.L.D.), a National Science Foundation Graduate Research Fellowship under Grant no. 1122374 (awarded to T.A.J.G.), a Helen Hay Whitney Fellowship (awarded to C.N), and funding from the MIT UROP office (B.B.). C.L.D. is a Howard Hughes Medical Institute Investigator. The work presented here is based upon research conducted at the Northeastern Collaborative Access Team beamlines, which are funded by the National Institute of General Medical Sciences from the National Institutes of Health (P41 GM103403). The Pilatus 6 M detector on 24-ID-C beamline is funded by a NIH-ORIP HEI grant (S10 RR029205). This research used resources of the Advanced Photon Source, a U.S. Department of Energy (DOE) Office of Science User Facility operated for the DOE Office of Science by Argonne National Laboratory under Contract No. DE-AC02-06CH11357.

References

1. Fujii K, Huennekens F (1974) Activation of methionine synthetase by a reduced triphosphopyridine nucleotide-dependent flavoprotein system. J Biol Chem 249: 6745–6753.
2. Knappe J, Schacht J, Möckel W, Höpner T, Vetter H Jr, Edenharder R (1969) Pyruvate formate-lyase reaction in *Escherichia coli*: The enzymatic system converting and inactive form of the lyase into the catalytically active enzyme. Eur J Biochem 11:316–327.
3. Broderick JB, Duffus BR, Duschene KS, Shepard EM (2014) Radical *S*-adenosylmethionine enzymes. Chem Rev 114:4229–4317.
4. Jarrett JT (2003) The generation of 5′-deoxyadenosyl radicals by adenosylmethionine-dependent radical enzymes. Curr Opin Chem Biol 7:174–182.
5. Harder J, Eliasson R, Pontis E, Ballinger MD, Reichard P (1992) Activation of the anaerobic ribonucleotide reductase from *Escherichia coli* by *S*-Adenosylmethionine. J Biol Chem 267:25548–25552.
6. Bianchi V, Reichard P, Eliasson R, Pontis E, Krook M, Jörnvall H, Haggård-Ljungquist E (1993) *Escherichia coli* ferredoxin NADP+ reductase: activation of *E. coli* anaerobic ribonucleotide reduction, cloning of the gene (fpr), and overexpression of the protein. J Bacteriol 175: 1590–1595.
7. Ifuku O, Koga N, Haze S-I, Kishimoto J, Wachi Y (1994) Flavodoxin is required for conversion of dethiobiotin to biotin in *Escherichia coli*. Eur J Biochem 224:173–178.
8. Bianchi V, Eliasson R, Fontecave M, Mulliez E, Hoover DM, Matthews RG, Reichard P (1993) Flavodoxin is required for the activation of the anaerobic ribonucleotide reductase. Biochem Biophys Res Commun 197: 792–797.
9. Brazeau BJ, Gort SJ, Jessen HJ, Andrew AJ, Liao HH (2006) Enzymatic activation of lysine 2,3-aminomutase from *Porphyromonas gingivalis*. Appl Environ Microbiol 72:6402–6404.
10. Cicchillo RM, Iwig DF, Jones AD, Nesbitt NM, Baleanu-Gogonea C, Souder MG, Tu L, Booker SJ (2004) Lipoyl synthase requires two equivalents of *S*-adenosyl-L-methionine to synthesize one equivalent of lipoic acid. Biochemistry 43:6378–6386.
11. Layer G, Verfurth K, Mahlitz E, Jahn D (2002) Oxygen-independent coproporphyrinogen-III oxidase HemN from *Escherichia coli*. J Biol Chem 277:34136–34142.
12. Grove TL, Ahlum JH, Qin RM, Lanz ND, Radle MI, Krebs C, Booker SJ (2013) Further characterization of Cys-type and Ser-type anaerobic sulfatase maturating enzymes suggests a commonality in the mechanism of catalysis. Biochemistry 52:2874–2887.
13. Grove TL, Lee K-H, St Clair J, Krebs C, Booker SJ (2008) In vitro characterization of AtsB, a radical SAM formylglycine-generating enzyme that contains three [4Fe-4S] clusters. Biochemistry 47:7523–7538.
14. Dowling DP, Bruender NA, Young AP, McCarty RM, Bandarian V, Drennan CL (2014) Radical SAM enzyme QueE defines a new minimal core fold and metal-dependent mechanism. Nat Chem Biol 10:106–112.
15. Bruender NA, Young AP, Bandarian V (2015) Chemical and biological reduction of the radical SAM enzyme CPH4 synthase. Biochemistry 54:2903–2910.
16. McCarty RM, Krebs C, Bandarian V (2012) Spectroscopic, steady-state kinetic, and mechanistic characterization of the radical SAM enzyme QueE, which catalyzes a complex cyclization reaction in the biosynthesis of 7-deazapurines. Biochemistry 52:188–198.
17. McCarty RM, Somogyi Á, Lin G, Jacobsen NE, Bandarian V (2009) The deazapurine biosynthetic pathway revealed: in vitro enzymatic synthesis of preQ0 from guanosine 5′-triphosphate in four steps. Biochemistry 48:3847–3852.
18. Bruender NA, Grell TA, Dowling DP, McCarty RM, Drennan CL, Bandarian V (2017) 7-Carboxy-7-deazaguanine synthase: a radical *S*-adenosyl-L-methionine enzyme with polar tendencies. J Am Chem Soc 139: 1912–1920.
19. Layer G, Moser J, Heinz DW, Jahn D, Schubert W-D (2003) Crystal structure of coproporphyrinogen III oxidase reveals cofactor geometry of radical SAM enzymes. EMBO J 22:6214–6224.
20. Vey JL, Drennan CL (2011) Structural insights into radical generation by the radical SAM superfamily. Chem Rev 111:2487–2506.
21. Vey JL, Yang J, Li M, Broderick WE, Broderick JB, Drennan CL (2008) Structural basis for glycyl radical formation by pyruvate formate-lyase activating enzyme. Proc Natl Acad Sci USA 105:16137–16141.
22. Dowling DP, Vey JL, Croft AK, Drennan CL (2012) Structural diversity in the AdoMet radical enzyme superfamily. Biochim Biophys Acta 1824:1178–1195.
23. Sancho J (2006) Flavodoxins: sequence, folding, binding, function and beyond. Cell Mol Life Sci 63:855–864.

24. Page CC, Moser CC, Chen X, Dutton PL (1999) Natural engineering principles of electron tunnelling in biological oxidation–reduction. Nature 402:47–52.
25. Hoover DM, Ludwig ML (1997) A flavodoxin that is required for enzyme activation: the structure of oxidized flavodoxin from *Escherichia coli* at 1.8 Å resolution. Protein Sci 6:2525–2537.
26. Minor W, Otwinowski Z. HKL2000 (Denzo-SMN) software package. Processing of X-ray diffraction data collected in oscillation mode, 1997 *Methods in Enzymology, Macromolecular Crystallography*. New York: Academic Press.
27. Sheldrick GM (2010) Experimental phasing with SHELXC/D/E: combining chain tracing with density modification. Acta Cryst D66:479–485.
28. Pape T, Schneider TR (2004) HKL2MAP: a graphical user interface for macromolecular phasing with SHELX programs. J Appl Cryst 37:843–844.
29. Terwilliger TC, Adams PD, Read RJ, McCoy AJ, Moriarty NW, Grosse-Kunstleve RW, Afonine PV, Zwart PH, Hung L-W (2009) Decision-making in structure solution using Bayesian estimates of map quality: the PHENIX AutoSol wizard. Acta Cryst D65:582–601.
30. Terwilliger TC, Grosse-Kunstleve RW, Afonine PV, Moriarty NW, Zwart PH, Hung L-W, Read RJ, Adams PD (2008) Iterative model building, structure refinement and density modification with the PHENIX AutoBuild wizard. Acta Cryst D 64:61–69.
31. Adams PD, Afonine PV, Bunkoczi G, Chen VB, Davis IW, Echols N, Headd JJ, Hung L-W, Kapral GJ, Grosse-Kunstleve RW, McCoy AJ, Moriarity NW, Oeffner R, Read RJ, Richardson DC, Richardson JS, Terwilliger TC, Zwart PH (2010) PHENIX: a comprehensive Python-based system for macromolecular structure solution. Acta Cryst D 66:213–221.
32. Emsley P, Cowtan K (2004) Coot: model-building tools for molecular graphics. Acta Cryst D60:2126–2132.
33. Chen VB, Arendall WB, Headd JJ, Keedy DA, Immormino RM, Kapral GJ, Murray LW, Richardson JS, Richardson DC (2010) MolProbity: all-atom structure validation for macromolecular crystallography. Acta Cryst D 66:12–21.
34. Morin A, Eisenbraun B, Key J, Sanschagrin PC, Timony MA, Ottaviano M, Sliz P (2013) Cutting edge: collaboration gets the most out of software. elife 2: e01456.
35. Schrödinger L (2010) PyMOL The PyMOL Molecular Graphics System. Version.
36. DeLano WL (2002) The PyMOL molecular graphics system. http://pymol.org.
37. Jurrus E, Engel D, Star K, Monson K, Brandi J, Felberg LE, Brookes DH, Wilson L, Chen J, Liles K (2018) Improvements to the APBS biomolecular solvation software suite. Protein Sci 27:112–128.
38. Atkinson HJ, Morris JH, Ferrin TE, Babbitt PC (2009) Using sequence similarity networks for visualization of relationships across diverse protein superfamilies. PloS one 4:e4345.
39. Smoot ME, Ono K, Ruscheinski J, Wang PL, Ideker T (2011) Cytoscape 2.8: new features for data integration and network visualization. Bioinformatics 27: 431–432.